Electronic and magnetic reconstructions in manganite superlattices

Kalpataru Pradhan, Arno P. Kampf

Electronic and magnetic reconstructions in manganite superlattices

Kalpataru Pradhan and Arno P. Kampf

Center for Electronic Correlations and Magnetism, Theoretical Physics III, Institute of Physics, University of Augsburg,
D-86135 Augsburg, Germany

We investigate the electronic reconstruction at the interface between ferromagnetic metallic (FM) and antiferromagnetic insulating (AFI) manganites in superlattices using a two-orbital double-exchange model including superexchange interactions, Jahn-Teller lattice distortions, and long-range Coulomb interactions. The magnetic and transport properties critically depend on the thickness of the AFI layers. We focus on superlattices where the constituent parent manganites have the same electron density, $n = 0.6$. The induced ferromagnetic moment in the AFI layers decreases monotonically with increasing layer width, and the electron-density profile and the magnetic structure in the center of the AFI layer gradually return to the bulk limit. The width of the AFI layers and the charge-transfer profile at the interfaces control the magnitude of the magnetoresistance and the metal-insulator transition of the FM/AFI superlattices.

I. INTRODUCTION

Correlated electron materials often involve the competition between various ordering tendencies of charge, orbital, spin, and lattice degrees of freedom. If further supplemented by weak disorder, cluster coexistence, percolative transport, and colossal response phenomena emerge. It therefore remains a continuing challenge to understand the functional properties of transition-metal oxides (TMOs).[1,2] The physics at the surface of TMOs is further enriched by atomic and electronic reconstructions and complicated by the lack of inversion symmetry.[3] When surfaces of two TMOs were joined together to form an interface,[4] new phenomena were discovered in the last decade. In some cases the phases at the interface are not even realized in the bulk of either of the TMOs which are joined together.[3,5] For instance, the discovery of the two-dimensional electron liquid[6] which forms at the interface between the insulators $LaAlO_3$ and $SrTiO_3$ started a new subfield in the research on oxide interfaces. Subsequent experiments revealed superconductivity,[7] ferromagnetism,[8] and even their coexistence.[9] These unexpected phases at interfaces pose fundamental physics questions and simultaneously bear promises of technological importance for the design of novel materials.[10]

The perovskite manganese oxides are a particularly remarkable example for the mutual coupling of electronic and lattice degrees of freedom.[11–13] The manganites $RE_{1-x}AE_xMnO_3$, where RE and AE denote rare- and alkaline-earth elements, respectively, are known for their colossal magnetoresistance.[14] The various phases in manganites with charge, orbital, and magnetic order have been elaborated for different combinations of RE and AE elements and doping regimes x.[2,11,15,16] The recent development in superlattices has created yet another tool to explore electronic and magnetic phases of manganites.

$La_{1-x}Sr_xMnO_3$, a solid solution of $LaMnO_3$ (LMO) and $SrMnO_3$ (SMO) exhibits a number of phases depending upon the doping concentration x. In addition to A-type at $x = 0$ and G-type antiferromagnetism at $x = 1$[17] also ferromagnetic and C-type antiferromagnetic (AF) phases exist at low temperature in an intermediate doping regime. For example, $La_{0.67}Sr_{0.33}MnO_3$ is a ferromagnetic metal and $La_{0.33}Sr_{0.67}MnO_3$ is an AF insulator.[16,18,19] In manganite superlattices $2m$ layers of LMO are deposited on m layers of SMO,[20,21] or vice versa.[22] For $m = 1$, LMO_{2m}/SMO_m and LMO_m/SMO_{2m} are the superlattice counterpart of the $La_{0.67}Sr_{0.33}MnO_3$ and $La_{0.33}Sr_{0.67}MnO_3$ manganites, respectively.

For LMO_{2m}/SMO_m superlattices the uniform ferromagnetic metallic (FM) behavior of the solid solution is recovered for $m \leqslant 2$. A metal-insulator transition (MIT) occurs for $m \geqslant 3$ accompanied by a strongly modulated magnetic structure across the interface.[20,21] Similarly, LMO_m/SMO_{2m} shows a C-type AF phase for $m = 1$ and $m = 2$ that exist in the solid solution counterpart $La_{0.33}Sr_{0.67}MnO_3$. The Néel temperature 250 K of the solid solutions increases to 320 K for $m = 1$. For $m \leqslant 2$, charge transfer from LMO to SMO may retain properties similar to the solid solutions. In these two scenarios, the charge transfer is likely confined to one to three unit cells. For $m > 2$, the increasing distance between the interfaces limits the charge transfer to the near vicinity of the interface. Due to this charge confinement LMO and SMO regain their respective parent phases away from the interface.

Considerable progress has been achieved in describing the modulated magnetic structure[23–27] and the MIT[27] in the LMO/SMO superlattices. The standard two-orbital double exchange model for manganites was implemented to calculate the average electron density for each layer of the LMO/SMO superlattices; away from the interface LMO and SMO layers regain their initial electron densities. The electron-density profile across the interface is determined by electrostatics with an electron transfer from the LMO to the SMO side. The magnetic profile for each layer follows the bulk phase diagram at the corresponding local density along with a weak proximity effect.[23,27]

In the initial studies of manganite superlattices[28–31] the primary intent was to improve the tunneling magnetoresistance[32,33] in a FM/AFI superlattice where the constituent parent FM and AFI manganites have the same electron density, $n = 1 - x$. FM/AFI superlattices with different combinations of manganites (FM = $La_{0.67}Sr_{0.33}MnO_3$ (LSMO), $La_{0.67}Ca_{0.33}MnO_3$ (LCMO),

$Pr_{0.67}Ca_{0.33}MnO_3$ (PCMO), $Gd_{0.67}Ca_{0.33}MnO_3$ (GdCMO); $n = 0.67$)[30,34–36] have been studied in recent years. The observed induced ferromagnetic moment in the AFI layers depends on their width and the induced moment is tunable by an external magnetic field.[30,36,37] Remarkably the required external field is much smaller than the magnetic field required to induce ferromagnetism in the parent AFI compound. This results in a large magnetoresistance in the FM/AFI superlattices which are therefore candidate materials for colossal magnetoresistance at room temperature. Manganite trilayers can also be used to design an efficient spin valve.[38]

In this paper, we have studied in detail the electronic and magnetic reconstructions in FM/AFI superlattices at electron density $n = 0.6$ for different widths of the AFI layers. Electrons are transferred from the FM to the AFI layers at the interface even though the initial electron density in the bulk FM and bulk AFI are equal. Our study confirms the underlying one-to-one correspondence between the density profile and the magnetic profile in the superlattices. With increasing AFI layer width, the induced ferromagnetic moment in the AFI layers decreases monotonically and drives an MIT in the superlattices. In addition to the large magnetoresistance our calculations explain the observed temperature crossover between positive and negative magnetoresistance and the two ferromagnetic transitions observed in the superlattices.[30,36]

The paper is organized as follows: In Sec. II, we introduce the two-orbital model for bulk perovskite manganites. For superlattices we specify the essential modification by adding long-range Coulomb (LRC) interactions and briefly present the applied Monte Carlo technique. The parameter space of the FM/AFI manganite superlattices is discussed in Sec. III. Electronic and magnetic reconstructions at manganite interfaces are emphasized in Sec. IV while Sec. V is devoted to the MIT. Results with and without LRC interactions are compared in Sec. VI. In Sec. VII, various combinations of electron-phonon couplings for FM and AFI manganites are considered. The role of disorder at the interface is discussed in Sec. VIII, and conclusions are presented in Sec. IX.

II. REFERENCE MODEL FOR MANGANITES

We construct a two-dimensional model Hamiltonian for manganite superlattices composed of FM regions separated by AFI regions as

$$H = H_{FM} + H_{AFI} + H_{lrc}, \quad (1)$$

where both H_{FM} and H_{AFI} have the same reference Hamiltonian,[39–42]

$$H_{ref} = \sum_{\langle ij \rangle \sigma}^{\alpha\beta} t_{\alpha\beta}^{ij} c_{i\alpha\sigma}^{\dagger} c_{j\beta\sigma} - J_H \sum_i \mathbf{S}_i \cdot \boldsymbol{\sigma}_i + J \sum_{\langle ij \rangle} \mathbf{S}_i \cdot \mathbf{S}_j$$
$$- \lambda \sum_i \mathbf{Q}_i \cdot \boldsymbol{\tau}_i + \frac{K}{2} \sum_i \mathbf{Q}_i^2 - \mu \sum_{i\alpha\sigma} c_{i\alpha\sigma}^{\dagger} c_{i\alpha\sigma}. \quad (2)$$

Here, c and $c^{\dagger}$ are annihilation and creation operators for itinerant e_g electrons and α, β refer to the two Mn-e_g orbitals $d_{x^2-y^2}$ and $d_{3z^2-r^2}$ labeled as a and b, respectively. The kinetic-energy part involves the nearest-neighbor hopping of e_g electrons with amplitude $t_{\alpha\beta}^{ij} (t_{aa}^x = t_{aa}^y \equiv t, t_{bb}^x = t_{bb}^y \equiv$

$t/3, t_{ab}^x = t_{ba}^x \equiv -t/\sqrt{3}, t_{ab}^y = t_{ba}^y \equiv t/\sqrt{3})$,[40] where x and y denote the spatial directions on a square lattice. J_H is the Hund's rule coupling between t_{2g} spins $\mathbf{S}_i$ and the e_g electron spin $\boldsymbol{\sigma}_i$, and J is the AF superexchange between the t_{2g} spins. λ measures the strength of the electron-phonon coupling between the Jahn-Teller (JT) distortions, Q_{2i}, Q_{3i} and the orbital pseudospin operators $\tau_{i2} = \sum_{\sigma} (c_{ia\sigma}^{\dagger} c_{ib\sigma} + c_{ib\sigma}^{\dagger} c_{ia\sigma})$, $\tau_{i3} = \sum_{\sigma} (c_{ia\sigma}^{\dagger} c_{ia\sigma} - c_{ib\sigma}^{\dagger} c_{ib\sigma})$. Here Q_{2i} and Q_{3i} are the distortions corresponding to the normal vibration modes of the oxygen octahedron that remove the degeneracy of the e_g levels. The stiffness of the JT modes is denoted by K. The stiffness of the breathing mode distortion (Q_{1i}), which couples to the local electron density, is considerably larger than K and therefore in the adiabatic approximation the coupling to Q_{1i} is neglected[40] in the Hamiltonian Eq. (2).

We treat all t_{2g} spins and lattice degrees of freedom as classical,[43,44] and measure energies in units of the Mn-Mn hopping $t_{aa} = t$. In manganites t is approximately 0.2–0.5 eV.[11,45] The estimated value of the Hund's coupling is 2 eV,[46] i.e., much larger than t. For this reason we further adopt the limit $J_H \to \infty$, for which the e_g electron spin perfectly aligns along the local t_{2g} spin direction. The infinite Hund's rule coupling then naturally leads to redefine the spinless e_g electron operator as $c_{i\alpha} = \cos(\theta_i/2) c_{i\alpha\uparrow} + \sin(\theta_i/2) e^{-i\phi_i} c_{i\alpha\downarrow}$, where the polar angle θ_i and the azimuthal angle ϕ_i determine the t_{2g} spin orientation. In terms of the redefined e_g electron operators, the kinetic energy takes the simpler form

$$H_{kin} = - \sum_{\langle ij \rangle, \alpha\beta} \tilde{t}_{\alpha\beta}^{ij} c_{i\alpha}^{\dagger} c_{j\beta},$$

where $\tilde{t}_{\alpha\beta}^{ij}$ is defined as $\tilde{t}_{\alpha\beta}^{ij} = \Theta_{ij} t_{\alpha\beta}^{ij}$ with $\Theta_{ij} = \cos(\theta_i/2) \cos(\theta_j/2) + \sin(\theta_i/2) \sin(\theta_j/2) e^{-i(\phi_i - \phi_j)}$. The factor controls the magnitude of the hopping amplitudes due to the different orientation of t_{2g} spins at sites i and j.

We set $K = 1$ without loss of generality, because if the lattice variable Q is replaced by $\sqrt{K}Q$, λ can be simply renormalized as $\lambda/\sqrt{K}$. The length of the t_{2g} spins is set to $|\mathbf{S}_i| = 1$. In an external magnetic field a Zeeman coupling $H_{mag} = -\mathbf{h} \cdot \sum_i \mathbf{S}_i$ is added to the Hamiltonian.

The reference "manganite model" H_{ref} in two dimensions is constructed to reproduce the correct sequence of magnetic phases in the bulk limit.[42,47] The different phases that are captured at low temperature are an orbitally ordered insulator at $x = 0$,[41] a charge and orbital ordered ferromagnetic insulator at $x = 0.25$,[47] a ferromagnetic metal window around $x = 0.67$, the CE charge and orbital ordered insulator around $x = 0.50$, a magnetic two-dimensional A-type AF phase, and a G-type AF phase at $x = 1.00$.

The average electron density of the constituent FM and AFI manganites in the FM/AFI superlattices is fixed by choosing the same chemical potential μ throughout the superlattice. The LRC interaction between all the charges, essential to control the amount of charge transferred across the interface, is taken into account via a self-consistent solution of the Coulomb potentials ϕ_i at the mean-field level by setting[48]

$$\phi_i = \alpha t \sum_{j \neq i} \frac{\langle n_j \rangle - Z_j}{|\mathbf{R}_i - \mathbf{R}_j|} \quad (3)$$

in the long-range Coulomb part of the Hamiltonian,

$$H_{lrc} = \sum_i \phi_i n_i. \tag{4}$$

It is assumed that all the point charges Z_j from the background ions are fixed and confined to the Mn sites. $\langle n_j \rangle$ refers to the e_g electron density at the Mn site $\mathbf{R}_j$. The long-range interactions between the background point charges and the e_g electrons are thereby combined with the charge-neutrality condition in the superlattice. Alternatively the Coulomb potentials ϕ_i can be determined self-consistently by solving the Poisson equation[49] which is equivalent to solving Eq. (3).

The Coulomb interaction strength is controlled by the parameter $\alpha = e^2/\epsilon a t$ where ϵ and a are the dielectric constant and the lattice parameter, respectively. This mean-field level setup is the minimal basis to study the charge transfer across the interface;[23,25,26] it is also commonly used in the context of semiconductor interfaces.[50]

The background dielectric constant ϵ is order of 20 in manganites.[51,52] It includes the lattice and the atomic polarizability contributions only. The dipolar contribution from the charge-carrier motion and the associated screening is neglected to treat the absolute permittivities of FM and AFI manganites on equal footing.[52] For a lattice constant $a = 4\,\text{Å}$, $t = 0.5$ eV, and $\epsilon = 20$, the approximate value of α is 0.2. The screening length in two dimensions is larger than in three dimensions.[53] This is taken into account by choosing a larger dielectric constant in the two-dimensional (2D) model ansatz. Specifically we use $\alpha = 0.1$ in our calculations. The α values employed earlier in 3D model calculations were in the range 0.1–1,[23,25,26] while a much smaller value of α was used in one dimension.[54]

We apply an exact diagonalization scheme to the itinerant electron system for each configuration of the background classical variables of the t_{2g} spins and the lattice distortions. The classical variables are annealed by starting from a random configuration. At each temperature the annealing requires at least 2000 system sweeps, by visiting every site of the lattice sequentially and updating the system by a metropolis algorithm. For each system sweep the computation time scales as $O(N^4)$ where N is the number of lattice sites. With thousands of annealing sweeps at various temperatures this procedure is time consuming.

We instead resort to a Monte Carlo sampling technique based on the "traveling cluster approximation" (TCA).[55] The TCA uses a moving cluster of size N_c constructed around the site of the Monte Carlo update. The computational cost thereby decreases to $O(N N_c^3)$ and allows us to treat system sizes up to $\sim 40 \times 40$, with an 8×8 moving cluster. The method and the associated transport calculations for $N = 24 \times 24$ were extensively benchmarked and successfully applied in several earlier studies.[41,42,47] At each system sweep we additionally solve for the Coulomb potentials ϕ_i in H_{lrc} self-consistently until the electron density at each site is converged. The maximum relative error for the convergence of the electron density is set to 0.01 at low temperatures while it is relaxed up to 0.03 at higher temperatures. For each fixed set of parameters, the calculations start from ten different initial realizations of

the classical variables. All the physical quantities are averaged over the results for these ten starting configurations.

III. SUPERLATTICES OF FERROMAGNETIC METALS AND ANTIFERROMAGNETIC INSULATORS

Here we analyze specifically superlattices composed of FM and AFI manganites. Even with the above described simplifications in the model Hamiltonian we have to contend with manganite states at different doping x, AF superexchange strengths J, and different electron-phonon couplings λ. Also the proper choice of relevant parameters for the combination of ferromagnetic metals and AF insulators is not obvious. In addition, due to the slight structural and chemical mismatch between the parent FM and AFI manganites the parameters at the interface may be altered with respect to the bulk values.

To constrain the parameter space we select the FM and AFI manganites of equal electron density $n = 1 - x$. We choose $n = 0.6$ above half filling to address the existing experiments on manganite superlattices near $x = 1/3$. The AF superexchange couplings may vary depending on the different combinations of RE and AE ions. But for simplicity we will use the typical value $J = 0.1$,[56] for both the FM and the AFI manganites. With the choice of the electron density and the superexchange couplings we are left with the crucial parameter λ to differentiate between a FM and an AFI phase.

Alternatively λ can be fixed and the differentiation between the ferromagnetic metal and the AF insulator is achieved by varying J. This requires a larger value of J in the AF insulator, but it leaves the ambiguity for choosing modified superexchange couplings at the interface. Yet another possibility is to keep each parameter J and λ fixed and to use different hopping amplitudes on the two sides of the interface. Again we are left with the possible modifications for the hopping amplitude at and across the interface. Since the λ and J values are measured in units of t, a smaller t value is equivalent to the combinations of larger λ and J values or vice versa. Smaller and larger λ values are thereby closely related to the larger and smaller bandwidth manganites, respectively.

Here we consider two λ values to differentiate between the FM and the AFI manganites. For the parameters $J = 0.1$ and the density $n = 0.6$, the ground state is FM for $\lambda \equiv \lambda_M = 1.50$ while it is an AFI for $\lambda \equiv \lambda_I = 1.75$. The AFI phase at $n = 0.6$ is not a perfect charge and orbital ordered CE phase which is stable only at $n = 0.5$.[40,42] The AFI phase at $n = 0.6$ is inhomogeneous, it contains the CE-type zigzag ferromagnetic chains and local charge ordered regions as shown in Fig. 1(a).

We compute the "one point" distribution function of the lattice distortions, $P(Q) = \langle \frac{1}{N} \sum_i \delta(Q - |Q_i|) \rangle$ where N is the total number of sites, to compare them with the electron-density variations. The two peaks in Fig. 2(a) for the AFI at $T = 0.01$ indicate that the distortions have a bimodal distribution. The sites with a large distortion attract more electrons with a density increase to $n_i \sim 0.8$. So the spatial density pattern in Fig. 1(a) reflects simultaneously the large and small structural distortions. The single peak structure of $P(Q)$ for the FM indicates instead that there are distortions of similar strength on all sites, which facilitates the motion of the electrons and thereby supports the metallic character.
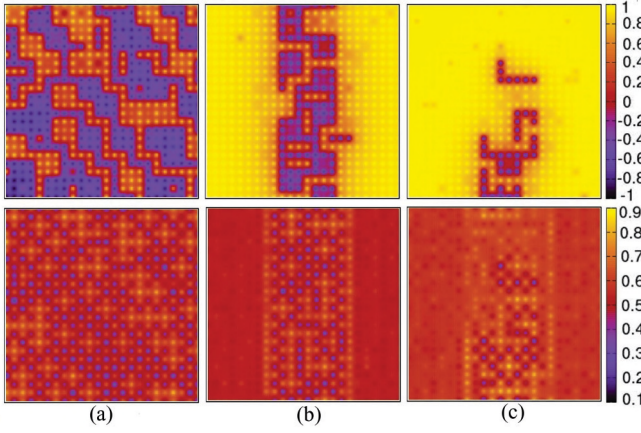
FIG. 1. (Color online) First row: The z components of the t_{2g} spins; second row: the electron density for each site on a 24×24 lattice at $T = 0.01$. (a) The parent AF insulator, (b) the superlattice with the width $w = 11$ of the AFI layer, (c) the superlattice with $w = 11$ in the presence of an external magnetic field, $h = 0.004$.

We obtain the resistivity for both FM and AFI bulk phases by calculating the dc limit of the longitudinal conductivity as determined by the Kubo-Greenwood formula,[57]

$$\sigma(\omega) = \frac{A}{N} \sum_{\alpha,\beta} (n_\alpha - n_\beta) \frac{|f_{\alpha\beta}|^2}{\epsilon_\beta - \epsilon_\alpha} \delta[\omega - (\epsilon_\beta - \epsilon_\alpha)], \quad (5)$$

with $A = \pi e^2/\hbar a$ and $n_\alpha = \theta(\mu - \epsilon_\alpha)$, a is the lattice spacing. $f_{\alpha\beta}$ denotes the matrix elements of the paramagnetic current operator $j_x = it \sum_{i,\sigma}(c^\dagger_{i+x,\sigma} c_{i,\sigma} - \text{H.c.})$ between eigenstates $|\psi_\alpha\rangle$, $|\psi_\beta\rangle$, and ϵ_α, ϵ_β are the corresponding eigenenergies. We extract the dc conductivity by calculating the "average" conductivity for a small low-frequency interval $\Delta\omega$ defined as

$$\sigma_{av}(\Delta\omega) = \frac{1}{\Delta\omega} \int_0^{\Delta\omega} \sigma(\omega) d\omega. \quad (6)$$

$\Delta\omega$ is chosen two to three times larger than the mean finite-size gap of the system as determined by the ratio of the bandwidth and the total number of eigenvalues. This procedure has been benchmarked in a previous work.[58] Figure 2(b) shows the temperature dependence of the resistivity $\rho = \sigma_{av}^{-1}$ in units of $\hbar a/\pi e^2$. The insulating behavior in the AFI at low temperatures is due to charge and orbital order, which opens an energy gap in the spectrum.
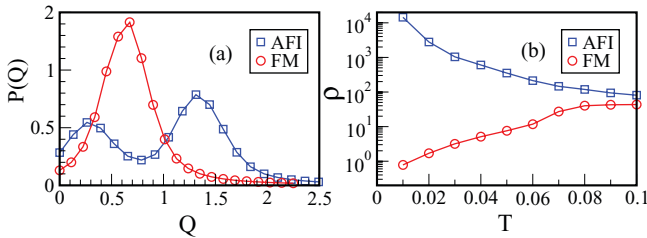

FIG. 2. (Color online) Bulk system at $n = 0.6$. (a) Distribution function for the lattice distortions $P(Q)$ of the bulk AFI ($\lambda_I = 1.75$) and bulk FM ($\lambda_M = 1.50$) at $T = 0.01$. (b) The resistivity variation with temperature for AFI and FM bulk systems.
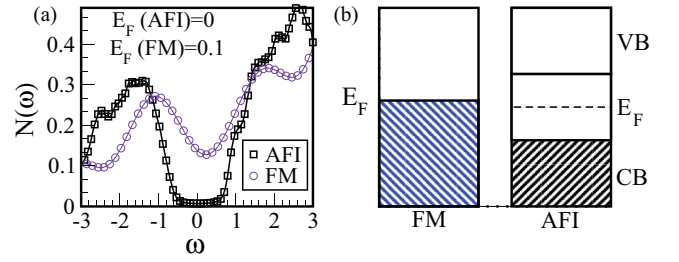

FIG. 3. (Color online) Bulk system at $n = 0.6$. (a) DOS of the bulk AFI ($\lambda_I = 1.75$) and FM ($\lambda_M = 1.50$) at $T = 0.01$. (b) Schematic energy diagram.

The density of states (DOS) $N(\omega) = \langle \frac{1}{N} \sum_\alpha \delta(\omega - \epsilon_\alpha) \rangle$ is shown in Fig. 3(a). The center of the gap in the DOS of the AFI state is chosen as the energy zero. With this choice the Fermi energy of the FM state at the same density is at $\epsilon_F = 0.1$. The DOS is finite for the FM state at its Fermi level. Figure 3(b) translates the results for the DOS into a schematic energy diagram. When the FM and the AFI manganites are joined together the DOS mismatch at the interface is expected to shift electrons from the FM to the AFI side. An FM/AFI superlattice is shown schematically in Fig. 4. The width of the middle AFI layer, sandwiched between the FM layers is denoted by w. Periodic boundary conditions are enforced in both directions and thereby represent a superlattice structure composed of alternating FM and AFI regions.

IV. CHARGE TRANSFER AND MAGNETIC RECONSTRUCTION AT THE INTERFACE

As we show below, if the width of the AF regions is small, they may become ferromagnetic and metallic in the superlattice structure. The induced magnetization is restricted to the near vicinity of the interfaces. The distance from the interface at which the parent AF insulating character is recovered depends upon the parameter α and the electron-phonon couplings λ_M and λ_I.

In this section we start with the specific choice of $\lambda_M = 1.50$, $\lambda_I = 1.75$, and $\alpha = 0.1$, and discuss results for the decrease of the magnetization with increasing width of the AFI layers. This decrease is quantified by the average z component of the t_{2g} spins $\langle S_z \rangle_I$ in the AFI layer, where the angular bracket
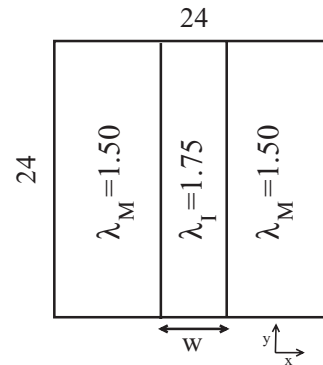

FIG. 4. Schematic view of the FM/AFI superlattice on a 24×24 lattice. We consider periodic boundary conditions in both directions.
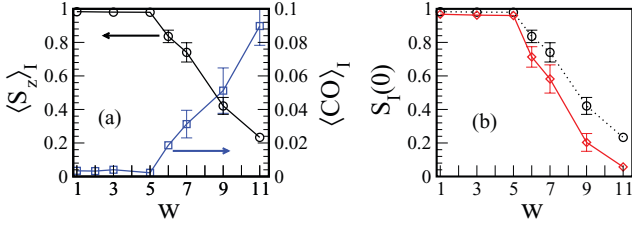
FIG. 5. (Color online) The average z component of t_{2g} spins $\langle S_z \rangle_I$ and the average staggered charge order $\langle CO \rangle_I$ (see text) in the AFI layer at $T = 0.01$. (b) Ferromagnetic structure factor $S_I(\mathbf{0})$ for different widths of the AFI layer at $T = 0.01$. The average z component is also replotted as the dotted line.

denotes the thermal average combined with an additional average over ten different "samples." We also define a measure for the local staggered charge order by $\langle CO \rangle_I = \frac{1}{N_I} \sum_{i \in AFI} \langle n_i \rangle e^{i(\pi,\pi)\cdot \mathbf{r}_i}$ for the AFI layer; i denotes one of the N_I lattice sites in the AFI layer with position $\mathbf{r}_i$. In Fig. 5(a), we plot $\langle S_z \rangle_I$ and $\langle CO \rangle_I$ for different widths w. For $w \leqslant 5$, the averaged $\langle S_z \rangle_I$ is near unity and starts to decrease for $w > 5$, while $\langle CO \rangle_I$ remains small for $w \leqslant 5$ and starts to rise for $w > 5$. Similarly [see Fig. 5(b)] also the long-wavelength magnetic structure factor $S_I(\mathbf{0})$ starts to decrease beyond $w = 5$, where $S_I(\mathbf{q}) = \frac{1}{N_I^2} \sum_{ij \in AFI} \langle \mathbf{S_i} \cdot \mathbf{S_j} \rangle e^{i\mathbf{q}\cdot(\mathbf{r}_i - \mathbf{r}_j)}$. So the decrease in the magnetization beyond a critical width w_c is accompanied by emerging charge order in the AFI layer. The critical width for fixed λ_I may change for a different set of parameters λ_M and α. This will be discussed in Secs. VI and VII. The critical width is therefore not directly related to an intrinsic length scale of the parent bulk AFI.

The averaged magnetization necessarily does not reveal any spatial variation transverse to the interface. In order to analyze the magnetization profile, we calculate the $\langle S_z(x) \rangle$ for each line of the superlattice with transverse coordinate x. Figure 6(a) shows the line averaged $\langle S_z(x) \rangle$ vs line index for $w = 7$. $\langle S_z(x) \rangle$ decreases for $x = 12$, 13, and 14, i.e., in the center lines of the AFI layer. So the induced ferromagnetic moment in the AFI layer is indeed confined to just the two lines nearest to the interface.

In the bulk for $\lambda_I = 1.75$ the AFI phase extends to electron densities larger than $n = 0.6$ and changes to a ferromagnetic insulating phase at $n = 0.75$.[47] It is therefore natural to explore the connection between the induced magnetization in the AFI layer with the electron densities at the interface. As shown in Fig. 6(b), at the interface the line averaged electron density $\langle n(x) \rangle$ of the FM layer decreases while $\langle n(x) \rangle$ for the AFI layer increases beyond the initial electron density 0.6. In fact $\langle n(x) \rangle$ at the fully magnetized lines $x = 10$ and 16 is nearly equal to 0.75.

The direction of electron transfer from the FM to the AFI regions was anticipated already in the discussion in Sec. III. Away from the interface the average electron density gradually returns to the initial electron density $n = 0.6$. In addition to the overall charge transfer, $\langle n(x) \rangle$ is spatially modulated perpendicular to the interface. These charge modulations are Friedel-like density oscillations; their amplitude decreases with the distance from the interface. The spatial density variations are nearly symmetric around the central line, $x =$
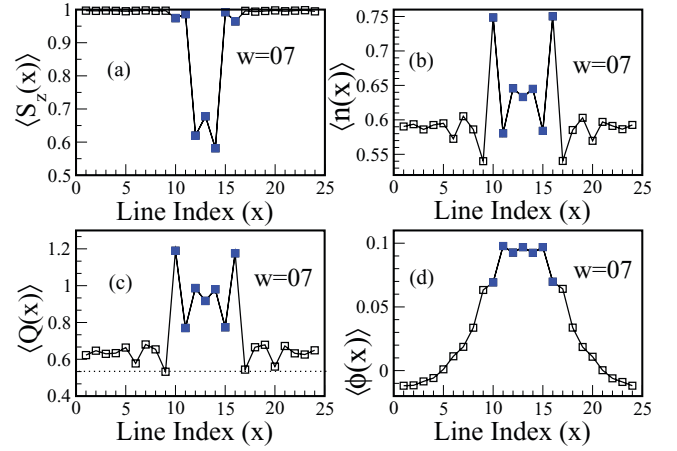

FIG. 6. (Color online) Line averaged (a) z component of the t_{2g} spins $\langle S_z(x) \rangle$, (b) electron density $\langle n(x) \rangle$, (c) LRC potentials $\langle \phi(x) \rangle$, and (d) lattice distortions $\langle Q(x) \rangle$ vs line index for $w = 7$. Open and closed symbols are for the FM and the AFI layers, respectively. The temperature is $T = 0.01$.

13. As we have verified, a perfect symmetry can be achieved by averaging over a larger number of samples.

For the incommensurate filling $n = 0.6$, the parent AFI is fragmented into small regions with and without charge and orbital order. High-density sites [see Fig. 1(a)] are always accompanied by large lattice distortions. Similarly a one-to-one correspondence between the electron densities and the lattice distortions exists in the superlattice. The line averaged lattice distortions $\langle Q(x) \rangle$ [see Fig. 6(c)] are in fact larger in the AFI layer. $\langle Q(x) \rangle$ is modulated similarly to the line averaged electron density shown in Fig. 6(b).

The amount of charge transfer from the FM to the AFI layers is controlled by the LRC interactions. The line averaged Hartree potential $\langle \phi(x) \rangle$ in Fig. 6(d) is negative for $x \leqslant 4$ and $x \geqslant 22$. The average electron densities for those lines is nearly equal to the initial electron density $n = 0.6$. The charge transfer is restricted to a few lines near the interface where the averaged potentials $\langle \phi(x) \rangle$ are positive, and thereby counteracts further electron transfer. Since ϕ_i and n_i are the self-consistent solutions of the Poisson equation, the increase or the decrease of the averaged electronic density has a one-to-one correspondence to the negative or positive curvature of $\langle \phi(x) \rangle$.

For $\alpha = 0.1$, see Fig. 7(a), the electron densities are clearly lower (higher) in the AFI (FM) layer as compared to $\alpha = 0$. The difference in the electron densities for $\alpha = 0$ and 0.1 is small due to the same initial electron density in the constituent FM and AFI manganites. This is in contrast to the quantitatively more important influence of LRC interactions at interfaces where the initial electron densities of the materials in contact significantly differ.[25] The LRC potentials decrease the electron density in the center of the AFI layer, but the average electron densities for individual lines at $x = 12$, $x = 13$, and $x = 14$ are still enhanced due to the Friedel-like density oscillations. The electron density in the central line $x = 13$ results from the superposition of the oscillations originating from $x = 10$ and $x = 16$. The constructive superposition is more pronounced for the AFI layer width $w = 5$ shown in Fig. 7(b), for which the center line is fully magnetized due
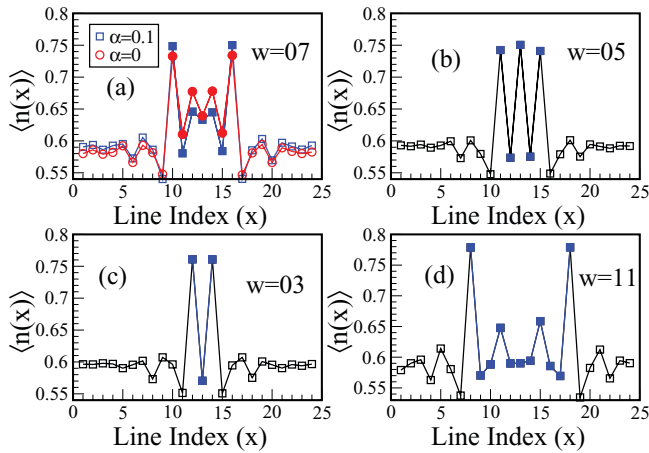
FIG. 7. (Color online) Line averaged electron density $\langle n(x) \rangle$ for (a) $w = 7$ with ($\alpha = 0.1$) and without ($\alpha = 0$) LRC interaction, (b) $w = 5$, (c) $w = 3$, (d) $w = 11$. Open and closed symbols are for the FM and the AFI layers, respectively. The temperature is $T = 0.01$.

to the enhanced electron density and the induced magnetism originating from the neighboring magnetized $2 + 2$ interfacial lines (two lines from each of the FM/AFI interfaces). For $w = 3$, in Fig. 7(c), the electron density of the central line is nearly equal to the initial electron density and the charge transfer is truly confined to the interface. For $w > 7$, density oscillations in the AFI layer disappear due the recovery of the bulk AFI character [see Fig. 7(d) for $w = 11$].

V. METAL-INSULATOR TRANSITION

In this section we compare the magnetic structure factor $S_I(\mathbf{0})$ in the AFI layer with the resistivity for the superlattice for current flow perpendicular to the interface. Figure 8(a) shows the temperature dependence of $S_I(\mathbf{0})$ in the AFI layer for
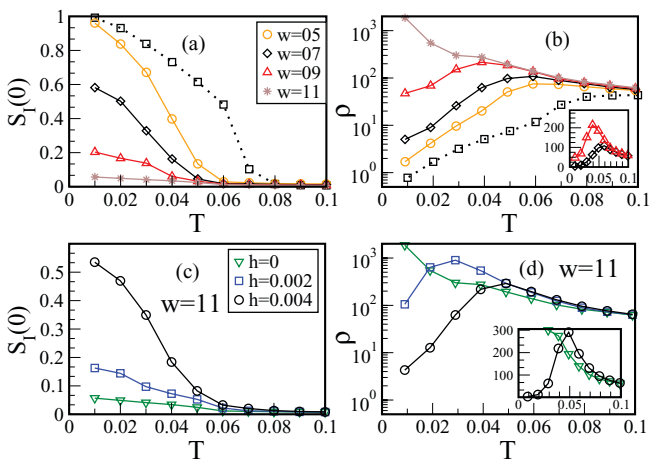

FIG. 8. (Color online) Temperature dependence of (a) the ferromagnetic structure factor $S_I(\mathbf{0})$ and (b) the resistivity ρ for different widths of the AFI layer. The dotted lines in (a) and (b) are for the bulk FM. (c) $S_I(\mathbf{0})$ and (d) resistivity variation with temperature for $w = 11$ in the presence of the external magnetic fields $h = 0.002$ and 0.004. Insets in (b) and (d) show the resistivity variation in the linear temperature scale.

different layer width w. For all temperatures, the ferromagnetic structure factor and the onset temperature for ferromagnetism decrease with increasing w. The z component of the t_{2g} spins $\langle S_{zi} \rangle$ and the electron densities for each site in the superlattice are shown in Fig. 1(b) for $w = 11$. The two lines in the AFI layer nearest to the interface are aligned ferromagnetically to the t_{2g} spins on the FM side in accordance with the discussion in Sec. IV. The magnetic structure of the center lines is already similar to the bulk AFI phase, and the density profile reveals the emergence of local charge ordering patterns in the AFI layer. The superlattice for $w = 11$ is therefore likely to be an insulator.

Figure 8(b) displays the temperature dependence of the longitudinal resistivity ρ of the superlattice. ρ for $w = 11$ steeply rises towards low temperatures as expected for an insulator. For $w \leqslant 7$, the superlattice is ferromagnetic and metallic at low temperatures. For $w = 5$, the onset temperature for ferromagnetism in the AFI layer is near 0.05, and simultaneously the resistivity starts to decrease.

The low-temperature resistivity increases monotonously with the AFI layer width. An MIT occurs beyond a threshold width similar as in the experiments by Li *et al.*[30] who measured the variations in the resistivity in LCMO/PCMO superlattices for different widths of the PCMO layer. In addition, the inset in Fig. 8(b) shows a hump in the resistivity for $w = 9$ and $w = 7$ at the ferromagnetic onset temperatures $T \simeq 0.04$ and 0.05, respectively, while there is no such hump in the bulk FM manganite [see the dashed line of Fig. 8(b)]. The humps in the resistivity curves increase and shift to lower temperatures with increasing AFI layer width (for $w \leqslant 9$). This trend agrees well with the LCMO/PCMO superlattice experiment[30] with the exception of the experimentally observed hump in the bulk FM limit. The temperature dependence of ρ near the MIT in bulk FM manganites is tied to the presence of intrinsic inhomogeneities and disorder.[59,60] Here we have not included any disorder[42] in the Hamiltonian; the MIT in the FM/AFI superlattice has a different origin. It is due to the induced onset of ferromagnetism in the AFI layer.

The natural next step is to explore the effect of an external magnetic field on the MIT in the superlattice. Figure 8(d) shows that the resistivity for $w = 11$ is lowered by the magnetic field at low temperatures. The connection between the resistivity decrease and the onset of ferromagnetism in the AFI layer is verified in Fig. 8(c). The MIT for $h = 0.004$ is at $T \simeq 0.05$; above this temperature, the resistivity is larger than the resistivity calculated for $h = 0$. The magnetoresistance, $[\rho(h) - \rho(0)]/\rho(0)$, therefore changes sign near the onset temperature for ferromagnetism.

At higher temperatures, the t_{2g} spins are randomly oriented. We recall that in the limit $J_H \rightarrow \infty$ the e_g electron spins are perfectly aligned along the local t_{2g} spin direction, so the current is equally carried by up-spin and down-spin electrons. In the presence of a weak external magnetic field, the number of e_g electrons is increased in the up-spin channel only in the FM layers and the tunneling current from the down-spin channel is decreased. The up-spin channel in the AFI layer remains unaltered and restricts the possible enhancement of the tunneling current from the up-spin channel. This results in an overall increase of the resistivity and a positive magnetoresistance.

At low temperatures in an external magnetic field the t_{2g} spins in the AFI layer tend to align in the same direction as the t_{2g} spins in the FM layers. So the tunneling current in the down-spin channel decreases but it increases for the up-spin channel. This decreases the overall resistivity of the superlattice. The corresponding crossover of the magnetoresistance from negative to positive was indeed reported in La$_{0.7}$Ce$_{0.3}$MnO$_3$/SrTiO$_3$-Nb (Ref. 61) and La$_{0.82}$Ca$_{0.18}$MnO$_3$/SrTi$_{0.95}$Nb$_{0.05}$O$_3$ (Ref. 62) heterojunctions.

The z component of the t_{2g} spins and the electron densities for each site in the superlattice are shown in Fig. 1(c) for $w = 11$ and $h = 0.004$. Ferromagnetic and AF structures coexist spatially separated in the AFI layer. The ferromagnetic phase in the upper panel is directly connected to the charge disordered regions in the lower panel. A magnetic field $h \geqslant 0.007$ is required to tune the parent AFI into a ferromagnetic metal. Lower fields are instead required for the FM/AFI superlattices which are therefore candidates to design materials with large magnetoresistance.

VI. RESULTS WITHOUT LRC INTERACTIONS

In order to analyze the effect of the LRC interactions we examine the ferromagnetic structure factor $S_I(\mathbf{0})$ for $\alpha = 0$ in Fig. 9(a). The critical width, beyond which $S_I(\mathbf{0})$ starts to decrease, is $w_c = 7$. With the LRC potentials, $\alpha = 0.1$, the critical width $w_c = 5$, as discussed in Sec. IV, is smaller due to the decrease in the average electron density in the AFI layer which is evident in Fig. 7(a). All the discussions in the previous two sections remain qualitatively valid also for $\alpha = 0$, but with a larger critical width w_c.

In Fig. 9(b), we plot the temperature dependence of $S_I(\mathbf{0})$ in the AFI layer for $\alpha = 0$. Similar to the results in Fig. 8(a), the onset temperature for ferromagnetism decreases with increasing w. Figure 9(c) shows the temperature dependence

of the longitudinal resistivity of the superlattice. For $w = 13$ and $w = 15$, the low-temperature resistivity rises by orders of magnitude. The inset of Fig. 9(c) zooms into the MIT at intermediate temperatures on a linear scale. The humps in $\rho(T)$ decrease and shift to higher temperatures for $w < 11$.

The onset temperature of ferromagnetism is higher in the FM layers than the AFI layers as becomes obvious from the temperature dependent structure factor in Fig. 9(d). So there are two ferromagnetic transitions in the superlattice: the first at T_{c1} for ferromagnetism in the FM layers and the second for the global ferromagnetism at $T_{c2} < T_{c1}$. The rise in the resistivity ρ near the hump just below T_{c1} is apparently due to the onset of ferromagnetism in the FM layers. The rise in ρ is expected for the same reason as for positive magnetoresistance discussed in Sec. V. The downturn in ρ results from the onset of global ferromagnetism in the superlattices at T_{c2}. These two transition temperatures are also observed in the LCMO/PCMO superlattices.[30] The temperature dependence of the ferromagnetic structure factor in the bulk FM state is included as the dotted line in Fig. 9(d). The ferromagnetic onset temperature for the FM layers in the FM/AFI superlattices is lower than for the bulk.

VII. VARIATION OF λ_M AND λ_I

In this section we compare $S_I(\mathbf{0})$ for different combinations of electron-phonon couplings λ_M and λ_I. In the previous sections $\lambda_M = 1.5$ and $\lambda_I = 1.75$ were chosen. If λ_I is kept fixed and λ_M varies between 1.0 and 1.6, the ground state is ferromagnetic and metallic in the bulk limit at $n = 0.6$. The induced magnetization in the AFI layer changes little for $\lambda_M \leqslant 1.5$ and for different widths w [see Fig. 10(a)]. For $\lambda_M = 1.6$, however, $S_I(\mathbf{0})$ is reduced for $w \geqslant 5$. The difference results from the decrease in the electron density in the FM layers nearest to the interface as becomes evident from the comparison with the bulk phase at $n = 0.5$.[42] For $\lambda_M \leqslant 1.5$, the ground state at $n = 0.5$ is a ferromagnetic metal while it is a CE-type antiferromagnet for $\lambda_M = 1.6$. For $\lambda_M \leqslant 1.5$, the magnetization in the interfacial FM layers is not altered, even if the electron density decreases towards $n = 0.5$. But for $\lambda_M = 1.60$, ferromagnetic order becomes unstable at the interfacial lines. The smaller magnetization at the interfacial FM layers decreases the induced magnetization in the AFI layer for $w \geqslant 5$.
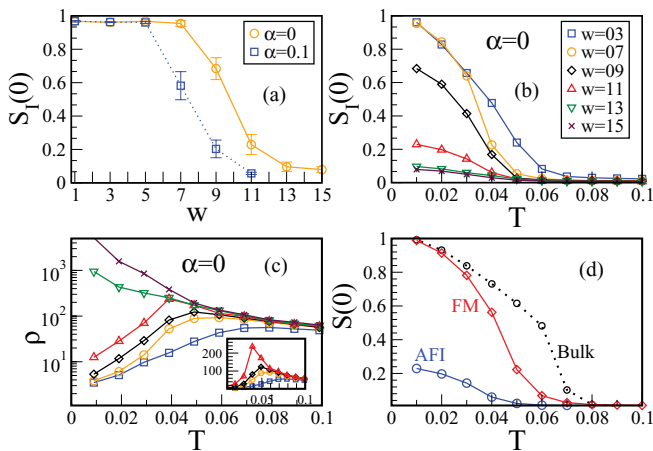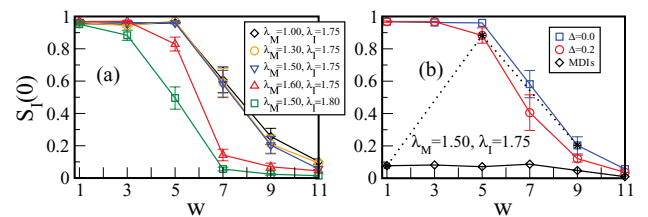

FIG. 9. (Color online) For $\alpha = 0$ (a) $S_I(\mathbf{0})$ for different widths of the AFI layers at $T = 0.01$. $S_I(\mathbf{0})$ for $\alpha = 0.1$ is also replotted as the dotted line. Temperature dependence of (b) $S_I(\mathbf{0})$ and (c) the resistivity for different widths of the AFI layers. Legends in (b) and (c) are the same. Inset in (c) shows the temperature dependence of the resistivity in the linear scale. (d) The temperature dependence of ferromagnetic structure factor for the AFI layer, the FM layer for $w = 11$, and the bulk FM.

FIG. 10. (Color online) $S_I(\mathbf{0})$ for different combinations of λ_M and λ_I values at $T = 0.01$. (b) $S_I(\mathbf{0})$ without ($\Delta = 0$) and with ($\Delta = 0.2$) quenched disorder, and with magnetically disordered interfaces (MDIs) (see text) for $\lambda_M = 1.50$ and $\lambda_I = 1.75$ at $T = 0.01$. The dotted line joins the three points, namely $w = 1$ (for MDIs), $w = 5$ (for $\Delta = 0.2$), and $w = 9$ (for $\Delta = 0$).

Figure 10(a) also indicates the reduced magnetization in the AFI layer for the larger electron-phonon coupling $\lambda_I = 1.8$, for which the AFI layer recovers the AF, charge ordered state at a smaller width w. It is therefore easier to induce a ferromagnetic moment in large-bandwidth (small λ) manganites. At $n = 0.67$, the bandwidth of PCMO is the largest among those manganites for which an AF, charge ordered insulating phase is experimentally observed.[16] In fact, in most of the experimental FM/AFI superlattices at $n = 0.67$ the insulating manganite PCMO is used along with a variety of different FM manganites.

VIII. DISORDER AT THE INTERFACE

The size mismatch of RE and AE elements in the manganites $RE_{1-x}AE_xMnO_3$ leads to tilting and distortions of the MnO_6 octahedra and variations in the local electronic parameters. The tilting and distortions of MnO_6 octahedra is generally known as A-type disorder. Here we have neglected the intrinsic A-type disorder in both the FM and the AFI manganites. Their interface is more prone to disorder due to chemical intermixing, lattice mismatch, and A-type disorder. We test the effect of quenched binary disorder in the terminating line of the FM layers at the interface by adding the potential disorder term by $\sum_j \epsilon_j n_j$ to the Hamiltonian. The sum over j is restricted to the terminating lines of the FM layers and ϵ_j is the quenched disorder potential with $\bar{\epsilon}_j = 0$ and values $\pm\Delta$.

In Fig. 10(b), we show the induced magnetization in the AFI layer for $\Delta = 0.2$ and different widths w, which apparently changes little between $\Delta = 0$ and $\Delta = 0.2$. All the discussions in the previous sections remain qualitatively unchanged for moderate disorder $\Delta = 0.2$. The magnetization of the interfacial lines of the FM layers, where Δ is included, is nevertheless likely to decrease for larger Δ. Ultimately the magnetization in those interfacial lines will be quenched due to spin disorder. In order to see the effect of the magnetically disordered interfaces on the AFI layer we have fixed randomly oriented spins in the interfacial lines throughout the Monte Carlo simulations. Indeed, in this extreme case, the induced magnetization in the AFI layer is very small [see Fig. 10(b)], irrespective of the AFI layer width. The magnetization of the FM layer at the interface is therefore crucial to induce the ferromagnetic moments in the AFI layer.

In the experiments it is apparently not clear whether or not there are magnetically disordered interfaces on the FM sides in the FM/AFI superlattices.[34] Thin AFI layers are likely to be more susceptible to disorder due to strain effects. The disorder strength Δ at the interface will therefore increase with decreasing the AFI layer width; the width dependence of the disorder strength is, however, hard to quantify. If we combine the results in Fig. 10(b) such that disorder strength is maximum for smaller AFI layers width and decreases thereafter for larger w (see the dotted line) then the magnetic moment in the AFI layer behaves non-monotonically which agrees qualitatively with the LSMO/PCMO superlattice experiment.[34] But more theoretical work is needed to understand this non-monotonic behavior.

IX. CONCLUSIONS

We have investigated the magnetic and electronic properties of 2D manganite superlattices at the specific electron density $n = 0.6$ using a two-orbital double-exchange model including superexchange interactions, JT distortions, and LRC interactions. At the interface electrons are transferred from the the FM to the AFI manganites. Friedel-like density oscillations are observed in both the FM and the AFI layers. Due to the charge transfer and the induced magnetization the smaller width AF insulator sandwiched between FM manganites turns into a ferromagnetic metal at low temperatures. The induced magnetization in the AFI layer decreases beyond a critical width and away from the interface the AFI layer gradually returns to the bulk AFI state. This results in an MIT in the FM/AFI superlattice driven by the AFI layer width. Only weak external magnetic field is required to tune the insulating into a metallic state. The sign of the magnetoresistance changes at higher temperatures. A remarkable result is that colossal magnetoresistance in manganite superlattices is achieved at lower magnetic fields as in the bulk phases of the constituent materials. For the range of AFI layer widths, at which FM/AFI superlattices show a metallic behavior at low temperatures, a hump in the temperature dependence of the resistivity ρ is observed. The hump in ρ is due to the presence of two ferromagnetic transition temperatures in the superlattice. The height of the hump decreases and shifts to higher temperatures with decreasing AFI layer width.

In summary, the width of the AFI layers controls the magnitude of the magnetoresistance and the MIT in the FM/AFI superlattices. Our 2D model Hamiltonian calculations provide a basis for explaining the two types of MIT in manganite superlattices: as a function of the AFI layer width and due to the presence of an external magnetic field. The non-monotonic behavior of the induced ferromagnetic moment in the AFI layer with increasing AFI layer width is traced to the effects of magnetic disorder at the interface. The electronic and magnetic reconstructions at the interface calculated using a 2D model are generally expected valid also for the more realistic 3D model. The change in the electron density at the interface for a 3D model calculation may, however, drive complex phases along the 2D interface with or without phase separation depending upon the initial electron densities of the constituent FM and AFI manganites. The extension of the presented calculation to an analogously defined 3D model is computationally more demanding but envisaged as a future project.

[1]E. Dagotto, Science **309**, 257 (2005).

[2]Y. Tokura, Rep. Prog. Phys. **69**, 797 (2006).

[3]H. Y. Hwang, Y. Iwasa, M. Kawasaki, B. Keimer, N. Nagaosa, and Y. Tokura, Nat. Mater. **11**, 103 (2012).

[4] J. Heber, Nature (London) **459**, 28 (2009).

[5] P. Zubko, S. Gariglio, M. Gabay, P. Ghosez, and J. M. Triscone, Annu. Rev. Condens. Matter Phys. **2**, 141 (2011).

[6] A. Ohtomo and H. Y. Hwang, Nature (London) **427**, 423 (2004).

[7] N. Reyren, S. Thiel, A. D. Caviglia, L. Fitting-Kourkoutis, G. Hammerl, C. Richter, C. W. Schneider, T. Kopp, A. S. Ruetschi, D. Jaccard, M. Gabay, D. A. Muller, J. M. Triscone, and J. Mannhart, Science **317**, 1196 (2007).

[8] A. Brinkman, M. Huijben, M. van Zalk, J. Huijben, U. Zeitler, J. C. Maan, W. G. van der Wiel, G. Rijnders, D. H. A. Blank, and H. Hilgenkamp, Nat. Mater. **6**, 493 (2007).

[9] D. A. Dikin, M. Mehta, C. W. Bark, C. M. Folkman, C. B. Eom, and V. Chandrasekhar, Phys. Rev. Lett. **107**, 056802 (2011).

[10] J. Mannhart and D. G. Schlom, Science **327**, 1607 (2010).

[11] *Colossal Magnetoresistive Oxides*, edited by Y. Tokura (Gordon and Breach, New York, 2000).

[12] *Colossal Magnetoresistive Manganites*, edited by T. Chatterji (Springer-Verlag, Berlin, 2004).

[13] E. Dagotto, *Nanoscale Phase Separation and Colossal Magnetoresistance: The Physics of Manganites and Related Compounds*, Springer Series in Solid State Sciences, Vol. 136 (Springer, Berlin, 2003).

[14] S. Jin, T. H. Tiefel, M. McCormack, R. A. Fastnacht, R. Ramesh, and L. H. Chen, Science **264**, 413 (1994).

[15] E. Dagotto, New J. Phys. **7**, 67 (2005).

[16] R. Kajimoto, H. Yoshizawa, Y. Tomioka, and Y. Tokura, Phys. Rev. B **66**, 180402 (2002).

[17] E. Wollan and W. Koehler, Phys. Rev. **100**, 545 (1955).

[18] J. Hemberger, A. Krimmel, T. Kurz, H. A. Krug von Nidda, V. Yu. Ivanov, A. A. Mukhin, A. M. Balbashov, and A. Loidl, Phys. Rev. B **66**, 094410 (2002).

[19] O. Chmaissem, B. Dabrowski, S. Kolesnik, J. Mais, J. D. Jorgensen, and S. Short, Phys. Rev. B **67**, 094431 (2003).

[20] A. Bhattacharya, S. J. May, S. G. E. te Velthuis, M. Warusawithana, X. Zhai, B. Jiang, J. M. Zuo, M. R. Fitzsimmons, S. D. Bader, and J. N. Eckstein, Phys. Rev. Lett. **100**, 257203 (2008).

[21] C. Adamo, X. Ke, P. Schiffer, A. Soukiassian, M. Warusawithana, L. Maritato, and D. G. Schlom, Appl. Phys. Lett. **92**, 112508 (2008).

[22] S. J. May, P. J. Ryan, J. L. Robertson, J.-W. Kim, T. S. Santos, E. Karapetrova, J. L. Zarestky, X. Zhai, S. G. E. te Velthuis, J. N. Eckstein, S. D. Bader, and A. Bhattacharya, Nat. Mater. **8**, 892 (2009).

[23] C. Lin and A. J. Millis, Phys. Rev. B **78**, 184405 (2008).

[24] B. R. K. Nanda and S. Satpathy, Phys. Rev. B **78**, 054427 (2008).

[25] R. Yu, S. Yunoki, S. Dong, and E. Dagotto, Phys. Rev. B **80**, 125115 (2009).

[26] L. Brey, Phys. Rev. B **75**, 104423 (2007).

[27] S. Dong, R. Yu, S. Yunoki, G. Alvarez, J. M. Liu, and E. Dagotto, Phys. Rev. B **78**, 201102(R) (2008).

[28] R. Cheng, K. Li, S. Wang, Z. Chen, C. Xiong, X. Xu, and Y. Zhang, Appl. Phys. Lett. **72**, 2475 (1998).

[29] I. N. Krivorotov, K. R. Nikolaev, A. Yu. Dobin, A. M. Goldman, and E. D. Dahlberg, Phys. Rev. Lett. **86**, 5779 (2001).

[30] H. Li, J. R. Sun, and H. K. Wong, Appl. Phys. Lett. **80**, 628 (2002).

[31] M. Jo, M. G. Blamire, D. Ozkaya, and A. K. Petford-Long, J. Phys.: Condens. Matter **15**, 5243 (2003).

[32] M. N. Baibich, J. M. Broto, A. Fert, F. Nguyen Van Dau, F. Petroff, P. Etienne, G. Creuzet, A. Friederich, and J. Chazelas, Phys. Rev. Lett. **61**, 2472 (1988).

[33] G. Binasch, P. Grünberg, F. Saurenbach, and W. Zinn, Phys. Rev. B **39**, 4828 (1989).

[34] D. Niebieskikwiat, L. E. Hueso, J. A. Borchers, N. D. Mathur, and M. B. Salamon, Phys. Rev. Lett. **99**, 247207 (2007).

[35] G. Lian, Z. Wang, J. Gao, J. Kang, M. Li, and G. Xiong, J. Phys. D **32**, 90 (1999).

[36] S. Mukhopadhyay and I. Das, Europhys. Lett. **83**, 27003 (2008).

[37] D. Niebieskikwiat, L. E. Hueso, N. D. Mathur, and M. B. Salamon, Appl. Phys. Lett. **93**, 123120 (2008).

[38] J. Salafranca, M. J. Calderon, and L. Brey, Phys. Rev. B **77**, 014441 (2008).

[39] S. Yunoki, T. Hotta, and E. Dagotto, Phys. Rev. Lett. **84**, 3714 (2000).

[40] E. Dagotto, T. Hotta, and A. Moreo, Phys. Rep. **344**, 1 (2001).

[41] S. Kumar, A. P. Kampf, and P. Majumdar, Phys. Rev. Lett. **97**, 176403 (2006).

[42] K. Pradhan, A. Mukherjee, and P. Majumdar, Phys. Rev. Lett. **99**, 147206 (2007).

[43] E. Dagotto, S. Yunoki, A. L. Malvezzi, A. Moreo, J. Hu, S. Capponi, D. Poilblanc, and N. Furukawa, Phys. Rev. B **58**, 6414 (1998).

[44] A. C. M. Green, Phys. Rev. B **63**, 205110 (2001).

[45] Z. Popovic and S. Satpathy, Phys. Rev. Lett. **88**, 197201 (2002).

[46] Y. Okimoto, T. Katsufuji, T. Ishikawa, A. Urushibara, T. Arima, and Y. Tokura, Phys. Rev. Lett. **75**, 109 (1995).

[47] K. Pradhan, A. Mukherjee, and P. Majumdar, Europhys. Lett. **84**, 37007 (2008).

[48] S. Okamoto and A. J. Millis, Phys. Rev. B **70**, 075101 (2004).

[49] S. Yunoki, A. Moreo, E. Dagotto, S. Okamoto, S. S. Kancharla, and A. Fujimori, Phys. Rev. B **76**, 064532 (2007).

[50] H. Lüth, *Surfaces and Interfaces of Solids* (Springer-Verlag, Berlin, New York, 1993).

[51] P. Lunkenheimer, V. Bobnar, A. V. Pronin, A. I. Ritus, A. A. Volkov, and A. Loidl, Phys. Rev. B **66**, 052105 (2002).

[52] J. L. Cohn, M. Peterca, and J. J. Neumeier, Phys. Rev. B **70**, 214433 (2004).

[53] B. Korenblum and E. I. Rashba, Phys. Rev. Lett. **89**, 096803 (2002).

[54] T. Oka and N. Nagaosa, Phys. Rev. Lett. **95**, 266403 (2005).

[55] S. Kumar and P. Majumdar, Eur. Phys. J. B **50**, 571 (2006).

[56] T. G. Perring, G. Aeppli, Y. Moritomo, and Y. Tokura, Phys. Rev. Lett. **78**, 3197 (1997).

[57] G. D. Mahan, *Quantum Many Particle Physics* (Plenum, New York, 1990).

[58] S. Kumar and P. Majumdar, Eur. Phys. J. B **46**, 237 (2005).

[59] J. Burgy, M. Mayr, V. Martin-Mayor, A. Moreo, and E. Dagotto, Phys. Rev. Lett. **87**, 277202 (2001).

[60] Y. Motome, N. Furukawa, and N. Nagaosa, Phys. Rev. Lett. **91**, 167204 (2003).

[61] Z. G. Sheng, W. H. Song, Y. P. Sun, J. R. Sun, and B. G. Shen, Appl. Phys. Lett. **87**, 032501 (2005).

[62] T. F. Zhou, G. Li, N. Y. Wang, B. M. Wang, X. G. Li, and Y. Chen, Appl. Phys. Lett. **88**, 232508 (2006).